A review of computer simulations of metal 3D printing

P. Ninpetch, P. Kowitwarangkul, S. Mahathanabodee, P. Chalermkarnnon, and P. Ratanadecho

View Online   Export Citation

ARTICLES YOU MAY BE INTERESTED IN
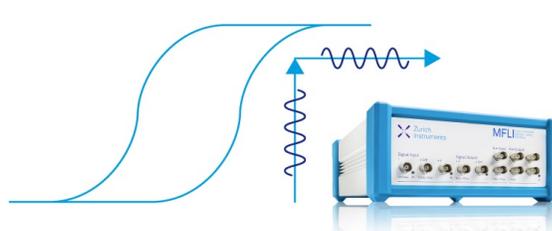
A Review of Computer Simulations of Metal 3D Printing

P. Ninpetch[1], P. Kowitwarangkul[1, a)], S. Mahathanabodee[2],
P. Chalermkarnnon[3] and P. Ratanadecho[4]

[1]The Sirindhorn International Thai-German Graduate School of Engineering (TGGS),
King Mongkut's University of Technology North Bangkok (KMUTNB) Bangkok, 10800, Thailand
[2]Department of Production Engineering, Faculty of Engineering,
King Mongkut's University of Technology North Bangkok (KMUTNB) Bangkok, 10800, Thailand
[3]Assistive Technology and Medical Devices Research Center,
National Science and Technology Development Agency (NSTDA), Pathum Thani 12120, Thailand
[4]Department of Mechanical Engineering, the Faculty of Engineering,
Thammasat University, Pathum Thani 12120, Thailand

a)Corresponding author: pruet.k@tggs.kmutnb.ac.th

Abstract. The metal 3D printing technologies are a joining materials process to create the metal 3D parts through CAD model, usually layer by layer, as opposed to subtractive manufacturing. This technology can be classified into four methods: selective laser melting (SLM), binder jetting, materials extrusion and direct energy deposition (DED). The process has advantages for producing near net shape parts, complex topology parts, lattice structure parts, manufacturing tool, medical parts, aerospace parts, and automotive parts. Over the last decade, the metal 3D printing simulation models were developed to investigate and predict the physical phenomena, thermo-mechanical behavior, and performance of metal 3D printing parts in the metal 3D printing technologies. The present study aims to review the computer simulation of metal 3D printing technologies. This review paper focuses on the numerical modelling and simulation in metal 3D printing process, recent simulation case studies and trends in metal 3D printing which are involved with the process parameters, temperature distribution, heat transfer, fluid dynamics, microstructure, porosity, melt pool characteristics and residual stress. The information obtained from this study will be useful for the further research studies in the metal 3D printing technologies.

INTRODUCTION ON METAL 3D PRINTING TECHNOLOGY

The metal 3D printing, also known as metal additive manufacturing (MAM) process, is becoming the next industrial revolution [1]. MAM is defined by American Society for Testing and Materials (ASTM) as a process of joining materials to make objects from 3D model data, usually layer upon layer, as opposed to subtractive manufacturing, e.g. milling, turning and drilling [2]. The advantages of the metal 3D printing include zero tooling, waste less, design freedom, producing near-net-shape parts, complex topology parts, lattice structure parts, and customization [3, 4]. The technology is used to build products in the various applications such as jig & fixture, mold and manufacturing tools, automotive parts, medical implant & healthcare, aerospace parts, lifestyle & sports, and customization parts [5]. The metal 3D printing can manufacture full density metallic parts from metal alloys e.g. titanium alloy, nickel-based superalloy, cobalt-chrome alloy, aluminium alloy, stainless steels and tool steels [6]. In 1997, Aero Mat can produce the first additive manufactured metal by using high-power laser to melt titanium alloy powder [7]. Figure 1 shows the comparison of additive manufacturing process and subtractive manufacturing process.

(a)

(b)
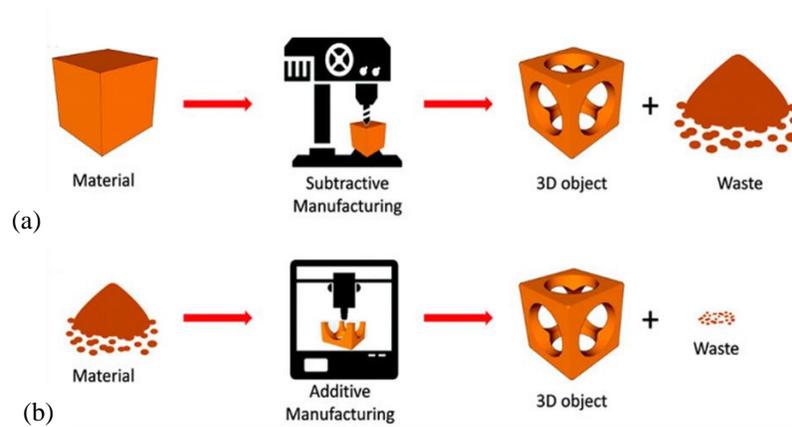
FIGURE 1. The comparison of (a) subtractive manufacturing process and (b) additive manufacturing process [8].

CLASSIFICATION OF METAL 3D PRINTING TECHNOLOGIES

The metal 3D printing technologies that are most widely used are selective laser melting (SLM) or laser powder bed fusion (L-PBF), electron beam melting (EBM), binder jetting, materials extrusion and direct energy deposition (DED) [7].

Selective Laser Melting (SLM) or Laser Powder Bed Fusion (L-PBF)

SLM process use laser as a heat source for fully melting metal powder to create 3D part layer fashion [5]. Figure 2 shows the schematic of SLM process. In this process, the powder bed is created by raking metal powder across the work space [9]. An energy source of laser is used to scan on each layer of metal powder bed to selectively melt the material according to the part cross section obtained from the CAD model. After one layer has been scanned, the piston under the product goes downward and the piston of the powder delivery goes upward by defined layer thickness. The cycle is repeated layer by layer, until the complete part is formed. Finally, the part is visible after the eliminated the excess metal powder from powder cake [5]. Usually the SLM process is conducted in an inert atmosphere such as argon or nitrogen for shielding of the molten metal.
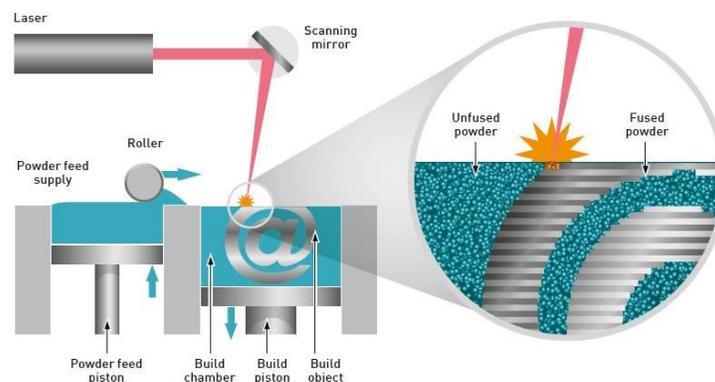

FIGURE 2. Schematic of laser powder bed fusion process [10].

Electron Beam Melting (EBM)

EBM process is similar to that of SLM process except the heat source, electron beam, for melting the metal powder [11]. The EBM process must be conducted in a vacuum atmosphere due to the limitation of the electrical

conductivity of material as shown in Fig. 3. The process is commonly applied for metallic applications, especially for complex designs.
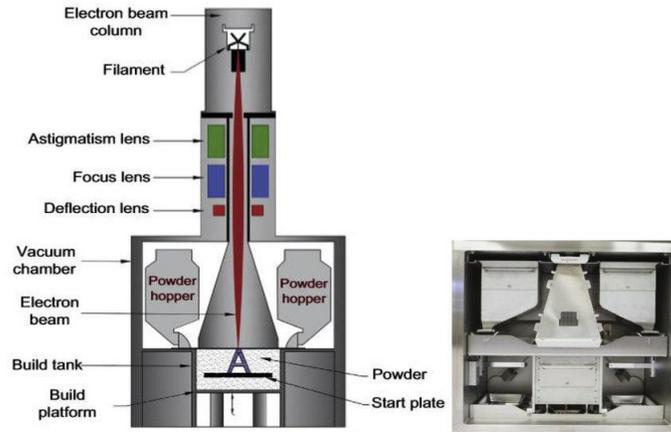
FIGURE 3. Schematic of electron beam melting process [12].

Material Extrusion

Material extrusion process has a similar operation method to that of metal injection molding (MIM). The process begins with mixing the metal powder with polymer binder. Then, the mixed material is extruded through the nozzle to create the 3D parts as layer-by-layer. The green body from this method needs to be sintered in an atmosphere furnace for near full density and strong mechanical properties [12]. The advantage of this technique is to provide a safe working environment where the operators can work without excess metal powder. Figure 4 shows the schematic of material extrusion process.
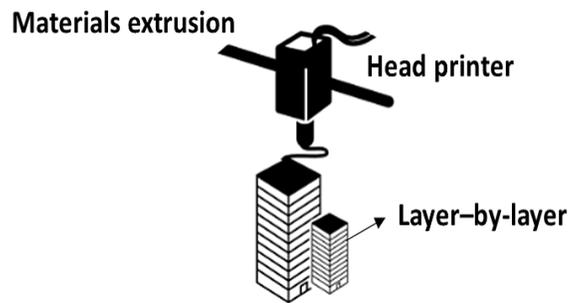
FIGURE 4. Schematic of material extrusion process [13].

Binder Jetting

The binder jetting technology is one of the main processes in metal additive manufacturing. This method works by creating metal powder across the work space with powder roller. Then, the polymer binder is dropped from print bar to the powder bed to produce the 3D object layer upon layer. Similar to material extrusion process, the green body needs to be sintered for densification [12]. This technology is used for printing the complex topology shape parts. The schematic of binder jetting process is shown in Fig. 5.
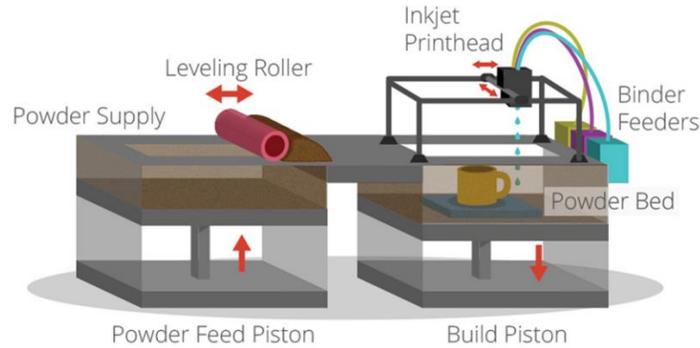
FIGURE 5. Schematic of binder jetting process [14].

Direct Energy Deposition (DED)

DED is a material joining process using the thermal energy heat source from electron beam or laser beam for melting the metal wire or powder. DED is generally used for large parts with manufacturing high performance super alloys [11]. This method can combine easily with conventional processes to complete machining. The metallic materials commonly used in the DED process are titanium, Inconel, stainless steel, aluminium and the related alloys for aerospace applications [12]. Figure 6 shows schematic of direct energy deposition processes: (a) powder fed, (b) wire fed.
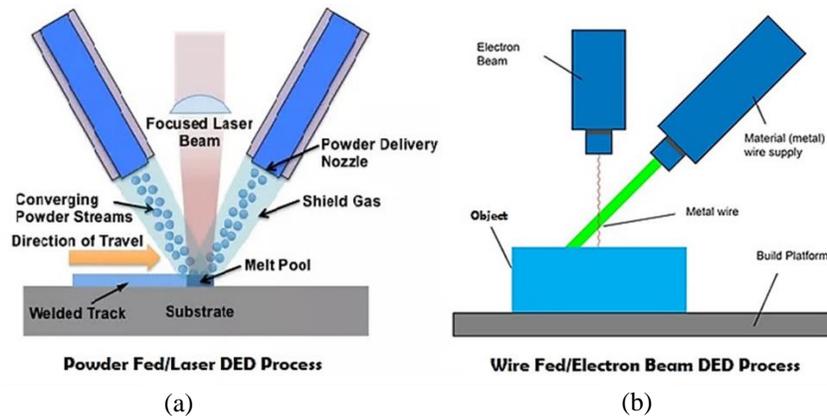

(a)   (b)

FIGURE 6. Schematic of direct energy deposition processes: (a) powder fed, (b) wire fed [15].

NUMERICAL MODELLING AND SIMULATION IN METAL 3D PRINTING

The numerical modelling and computer simulation are useful for investigation and prediction of the underlying physical phenomena, and thermal-mechanical behavior that can occur during the metal 3D printing process such as temperature distribution, heat transfer, melt pool dynamic, melt pool geometry, phase transformation, melting and solidification, Marangoni convection, microstructure evolution, residual stress, and distortion [16]. Figure 7 shows the typical of physical phenomena during metal 3D printing process. Currently, the numerical modelling can now support the metal 3D printing process in terms of SLM, direct metal laser sintering (DMLS), DED, and EBM [17, 18]. The numerical modelling and simulation provide a better understanding of designing parts, an ability to optimize production, lower manufacturing costs, knowledge to improve metal 3D printing processes [19]. In metal 3D printing process, the numerical modelling was modelled on multi-scale of length to explain several aspects of the process [16].
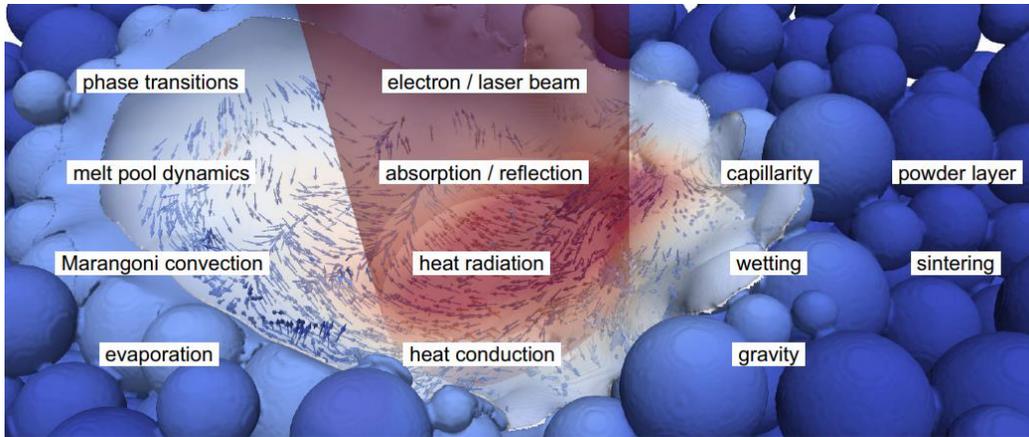
FIGURE 7. Typical of physical phenomena in metal 3D printing process [16].

A previous study [20] summarized that the computer simulation modelling in metal 3D printing has been classified into four levels including (1) micro-scale (10^{-9} m to 10^{-6} m), (2) particle scale (10^{-6} m to 10^{-3} m), (3) meso-scale (10^{-3} m), and (4) macro-scale (10^{-3} m to 1 m). The multi-scale modelling of the metal 3D printing process is illustrated in Fig. 8. The details of each level can be explained as follows:
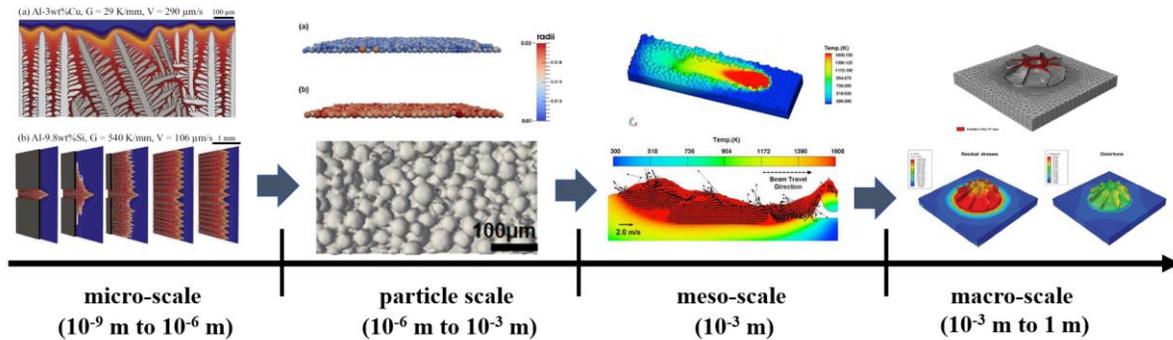

FIGURE 8. The multi-scale modelling of the metal 3D printing process [21-24].

## Micro-Scale Modelling (10^{-9} m to 10^{-6} m)

Micro-scale modelling, such as phase field modeling is carried out to predict the microstructure evolution during non-equilibrium condition with rapid cooling rate and effect of thermal cycle in metal 3D printing process [20]. It includes modelling of solidified materials, phase formation, solid state phase transformation, solidification segregation of alloys, grain structure, grain-oriented direction, etc. Radhakrishnan et al. [25] developed the large-scale phase field simulations of microstructure evolution during thermal cycling of Ti-6Al-4V. The study aimed at investigating the influence of the energy contributions from thermodynamics, interfacial energy and strain energy on the variant selection for different levels of undercooling and nucleation rate. They found that the phase field simulations are able to present the basket weave or colony structure formation when the transformation temperature. A prior research study [26] has established a two-dimensional numerical modelling to simulate the of grain structure evolution during the laser additive manufacturing process. The numerical modelling is based on the cellular automata (CA) and finite-difference (FD) methods. The CA method is used to analyze grain growth. The results from the study is in agreement with the experimental data describing the main characteristics of the grain structure. The model can be applied to predict and optimize the grain structure produced by the laser additive manufacturing technique [26]. Figure 9 shows the example of simulated microstructure of SLM steel (with each new powder layer the melt pool moves in the horizontal direction).
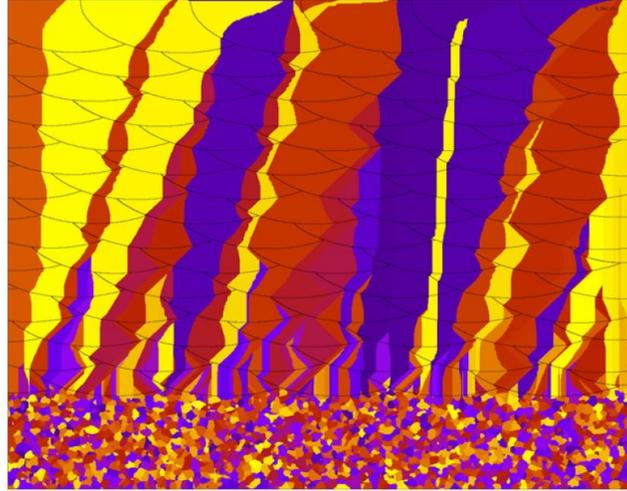
FIGURE 9. The example of simulated microstructure of SLM steel [26].

# Particle-Scale Modelling (10^{-6} m to 10^{-3} m)

The particle-scale modelling is a common model in SLM and EBM process. This numerical modelling was built to investigate particle interactions, particle distribution size, powder spreading, and particle packing density [27]. The discrete element method (DEM) was performed to simulate the motion of a large number of individual particles including contact interactions between particles and particles, and particles and walls [23]. The Discrete Element Method (DEM) is a numerical modelling process for simulating the behavior of both continuous and discontinuous material systems [28]. In the previous research [23], the powder particle packing model based on discrete element method (DEM) was used to study the simulation of powder packing. The powder particles are defined as elastic spheres with various radius. The powder container of the particles is provided as rigid walls. Individual particle has six velocity components three translational and three rotational in the x, y and z axis of a cartesian coordinate system. The Inconel 718 with spherical shape was used in the study. The two-particle size condition such as mean radius of 12.7 µm, and mean radius of 17.3 µm were considered in the study. Figure 10 illustrates the stack-up of powder particles calculated by using the DEM model with different particle size distributions (a) mean radius of 12.7 µm and (b) mean radius of 17.3 µm.
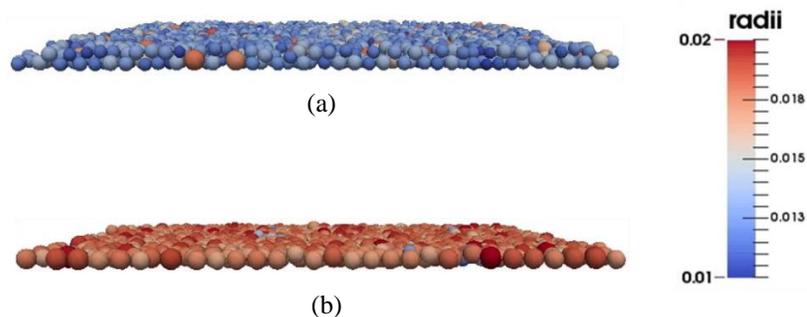
FIGURE 10. The stack-up of powder particles calculated by using the DEM model with different particle size distributions (a) mean radius of 12.7 µm and (b) mean radius of 17.3 µm [23].

Meso-Scale Modelling (10^{-3} m)

This scale is mainly used for the simulation of heat transfers, molten fluid flow, melting and solidification, Marangoni effect, and balling effect formation. In the SLM process, a complicate thermal history takes place in the metallic metal 3D printing part and involves with directional heat extraction, repeated rapid melting and rapid solidification [29, 30]. Heat transfer models are quite complex due to the laser scanning rates and the occurrence of phase transformations in a short period of time [31]. Heat transfer process consists of powder bed radiation, convection, and heat conduction inside the powder bed and between the powder bed and substrate. Fourier heat conduction, heat convection, and heat radiation models are most commonly used for the simulation of heat transfer process in SLM [32]. The model of fluid dynamics and Marangoni effect in SLM process is based on mass, momentum and energy conservation equations with the volume of fluid (VOF) method [23]. The VOF was utilized for tracking position and shape of the molten pool surface. The molten fluid flow is assumed to be incompressible and Newtonian with laminar flow [23]. In a previous research study [33], the model from [34] has been expanded to a three-dimensional model by considering the thermal behavior and fluid dynamics in the molten pool caused by buoyancy forces and Marangoni effect. Marangoni effect is the phenomena which relates to the mass transfer along an interface due to the surface tension gradient. In the melt pool, the strong temperature gradients at the laser hot spot cause surface tension which depends on temperature. Panwisawas et al. [22] developed the mesoscale modelling of SLM process to investigate and predict the effect of process parameters including layer thickness and scanning speed on the surface morphology of Ti-6Al-4V by using thermal fluid dynamics calculations. The material used in this study was Ti-6Al-4V powder in the size range of 20–50 μm. The single-track scanning was performed on powder layers with different thicknesses ranging from 20 μm up to 100 μm with laser power of 400W at scanning speed 2400 mm/s. They discovered that thermal fluid flow results of single scanned tracks are consistent with experimental study. The results suggest that the melted tracks become increasingly irregular shaped when the layer thickness and laser scanning speed increase. The surface morphology of single track with different layer thickness is shown in Fig. 11.
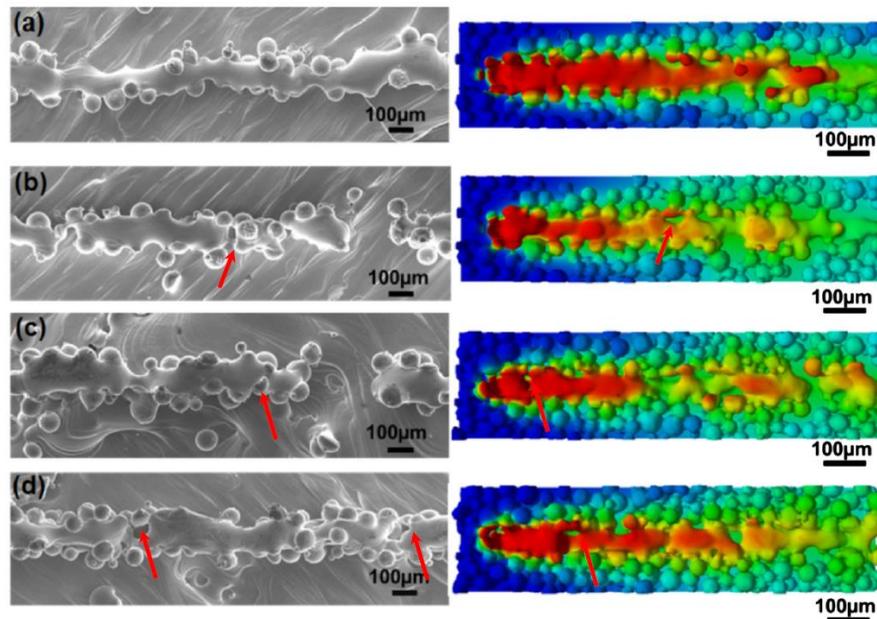

FIGURE 11. The surface morphology of single track with different layer thickness (a) 20 μm, (b) 60 μm, (c) 80 μm, (d) 100 μm with laser power of 400W and scanning speed 2400 mm/s [22].

Macro-Scale Modelling (10^{-3} m to 1 m)

The final level of numerical modelling and simulation of metal 3D printing process is macro-scale modelling. The utilization of this scale is to simulate and predict the thermal-mechanical behavior such as temperature distribution, residual stress, and distortion [21]. Modelling of this level is based on finite element analysis (FEA). Ninpetch [35] studied the effect of process parameters including laser power and scanning speed on the temperature distribution in the SLM process by using the commercial CFD software simulation Flow-3D (Flow-weld). The results suggest that at the higher laser power and lower scanning speed, the temperature field has a larger region of heat distribution than that of lower laser power and high scanning speed due to heat accumulation. Figure 12, 13 exhibits the effect of laser power and scanning speed on temperature distribution in SLM process.


Laser power = 120 W
Scanning speed = 0.4 m/s

Laser power = 140 W
Scanning speed = 0.4 m/s
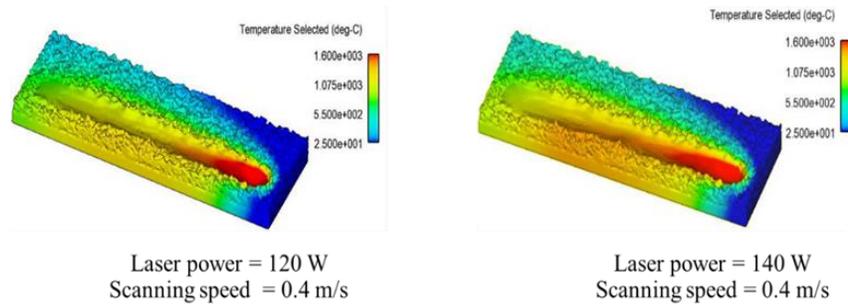
FIGURE 12. The effect of laser power on temperature field during SLM process [35].

Laser power = 120 W
Scanning speed = 0.4 m/s

Laser power = 120 W
Scanning speed = 0.6 m/s

Laser power = 120 W
Scanning speed = 0.8 m/s
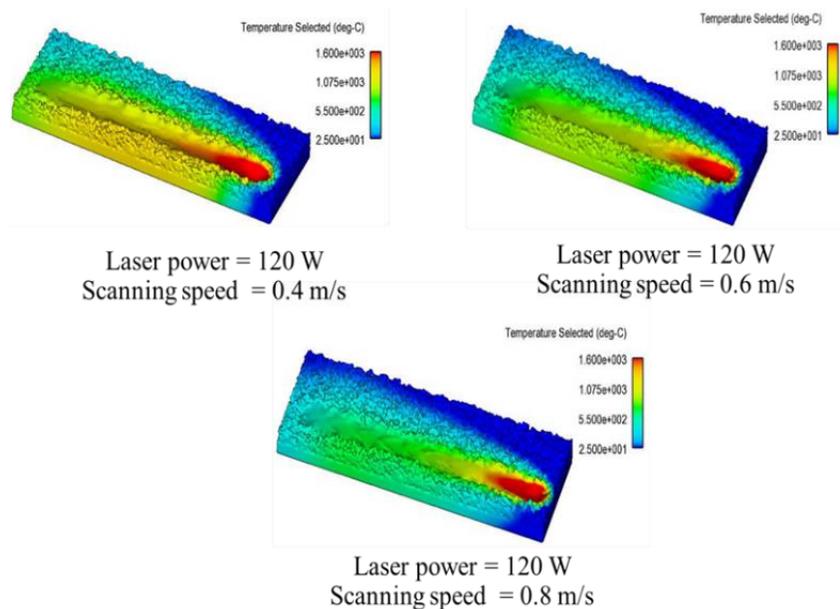
FIGURE 13. The effect of scanning speed on temperature field during SLM process [35].

Prabhakar et al. [36] developed the computational modeling to simulate residual stress formation in the EBM process within an Arcam machine for Inconel 718. Thermal and stress analyses are performed with the finite element analysis to observe the deformation and stresses in the tensile test specimen build and the base plate. The simulation results indicated that the warping in the base plate and the build occurred during the formation of the first few layers. Furthermore, the warping was also exposed during the cool down step. Figure 14 shows the computational results of the tensile test specimen build in the base plate in which the red contour depicts the effects of warping. [36]
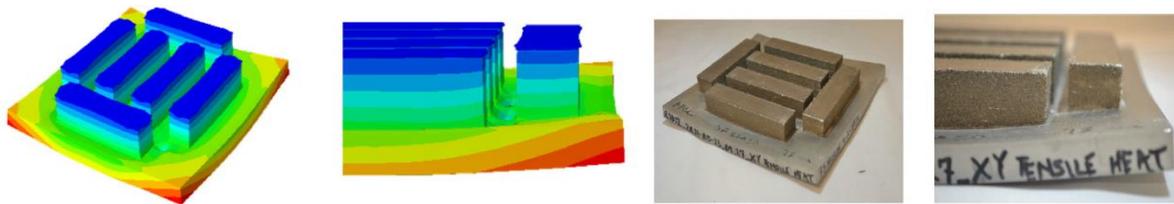
FIGURE 14. The computational results of tensile test specimen build showing the effects of warping [36].

Topology Optimization of Part Modelling

Besides the modelling mentioned above, one of the numerical modelling to design parts in metal 3D printing process is topology optimization. It is a mathematical method to provide the optimum distribution of material in a parts design for a given set of loading and boundary condition [37]. The model is based on FEA. This method is conducted by removing the material from the location where it is not essential to support the specific load or specific boundary condition. The final result of topology shapes, which resemble tree branches and bones obtained from this method are not constant in cross section [37]. The topology optimization modelling starts with creating a coarse 3D model and defining the specific load and boundary conditions into parts. The optimization software is then calculating all the constraint applied. After that, the dispensable regions will be eliminated. Final geometry with both mechanical and design requirements will be obtained [38]. Figure 15 shows the workflow step of topology optimization of part modelling.
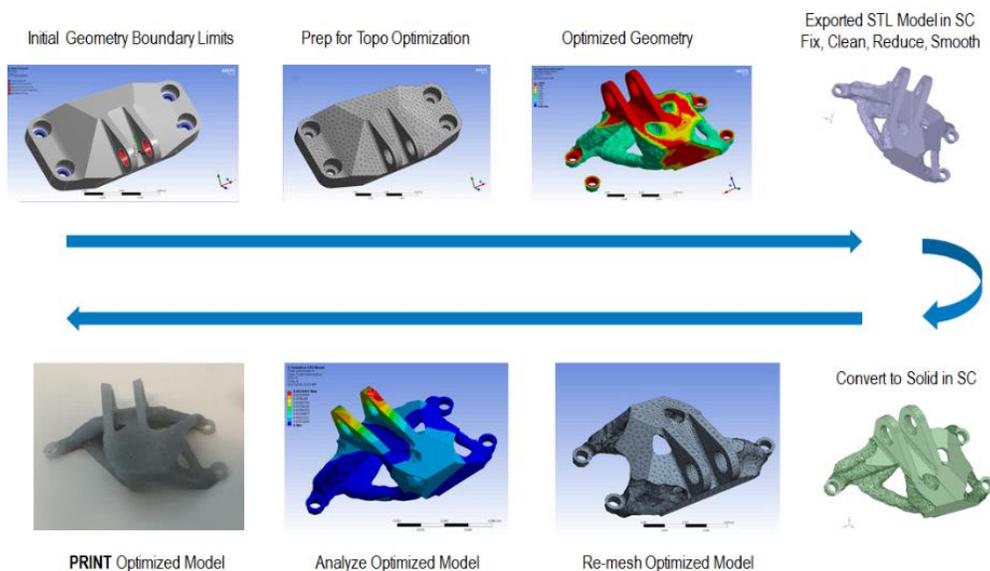
FIGURE 15. Workflow step of Topology optimization of part modelling [39].

CUTTING-EDGE METAL 3D PRINTING SIMULATION SOFTWARE

The simulation software is a valuable tool to gain the body of knowledge of several aspects in the metal 3D printing technologies [18]. This kind of software helps users to obtain the best orientation of parts, understand the

thermo-mechanical evolution, and predict distortion of parts in the metal 3D printing process [18]. Table 1. shows the list of cutting-edge metal 3D printing simulation software.

<p style="text-align:center">TABLE 1. The list of cutting-edge metal 3D printing simulation software [19].</p>

Software	Features
Ansys Additive print	- To design topology optimization, thermal analysis and lattice structures - To validate the design of metal parts - To create optimal support structures and generate distortion-compensated STL files. - To understand the properties of the final printed part.
Flow-3D / Flow-weld	- To simulate the powder distribution, the melting of powder, melt pool formation and solidification - To help the optimization printing parameters and provide a better understanding of powder microstructure.
COMSOL multiphysic	- To optimize the metal 3D printing process for metals. - To predict the mechanical and microstructural properties of the final product like final shape, deformation, and stress levels.
ESI Additive manufacturing	- To simulate manufacturing defects, residual stresses and porosity levels. - To predict the behavior of a final part quality (for example, surface roughness and distortions) after removal from the build platform.
GENOA 3DP	- To predict deformation, residual stress, and voids in parts produced additively. - To find optimal printing conditions - To predict fracture, failure type and percentage of contribution by a failure type
Additive Works' Amphyon	- To simulate various stages of the additive manufacturing process, from the printing process itself to post-processing steps, like the removal from the build plate and secondary heat treatment.
Simufact's Additive	- To identify the best build orientation, optimize support structures automatically and identify potential manufacturing issues. - To provide distortion compensation by defining tolerable deviations and then generating the geometry with the minimal deformation.
Autodesk's Netfabb	- To predict the thermal and mechanical behaviour of parts, identifying deformations in a virtual environment. - To performed on complex parts much faster than with local solvers.
Dassault Systèmes SIMULIA	- To predict part distortions, residual stresses, and microstructures in metal and composite parts.

THE INFLUENCE OF PROCESS PARAMETERS IN METAL 3D PRINTING PROCESS

The quality of final parts can be determined by various process parameters in the metal 3D printing technologies. The main process parameters are laser power, laser spot size, scanning speed, hatch spacing, layer thickness, scanning pattern, powder distribution, packing density, cooling rate and working atmosphere. During the metal 3D printing process, it involves several complex multiphysics such as the materials absorption, heat transfer, molten fluid dynamic, and phase transformation etc. These multiphysics have significant influence on the density, porosity, mechanical properties, microstructure, melt pool geometry, and residual stress of final parts. This section will discuss the effect of process parameters in metal 3D printing process.

The experimental results from previous research on porosity indicated that the density is increased with the less porosity inside the structure of metal 3D printing parts [40,41]. The porosity is decreased when the scan speed decreases and the laser power increases [42]. When increase layer thickness and hatch spacing showed that in porosity increases [43]. The melt pool shape is determined by laser process parameters and the thermal conditions near the melt pool [44]. The shape of melt pool can change from ellipse shape to tear drop shape when scanning speed is increased [45, 46]. It has an influence on the fusion zone grain structure. The geometric characteristics of laser melted tracks strongly depend on the laser process parameters and surface tension force of materials. Surface tension can be influenced by process parameters. [45]. X. Zhao et al. [47] used the experimental study to create a single melted track mapping with different laser power and scanning speeds of AISI 420 martensitic stainless steel. They summarized that (1) discontinues melted track with balling effect, (2) continue melted track, and (3) continue melted track with crack. The discontinuous track with balling effect can expose when the lower laser power and high scanning speed are applied. This phenomenon occurs due to the insufficient of laser energy heat source to fully melt the metal powder bed. The balling effect can be controlled by effect of process parameter such as laser power, scanning speed and the oxygen content in atmosphere. The continuous melted track can be formed when the properly laser process parameters are applied (e.g. higher laser power and slower scanning speed) [47]. The discontinuous track with fragment can be formed with the lower laser power and lower scanning speed. The laser melted track cannot completely melt and also caused high residual stress and cracks [47].

The width and depth of single melted track formation are increased when the higher laser power and lower scanning speed are applied [46, 48, 49, 50]. The experimental study [51, 52, 43] presents that the aperture between two neighboring tracks is increased and leads to separation with an increase of hatch spacing. The superior mechanical properties of final parts occur when the properly process parameters are applied [7]. The tensile strength of metal 3D printing parts is an anisotropy behavior. The results from [7, 53] reveal that horizontally built direction of SLM parts showed better ductility and vertically built direction showed a proper combination of strength and ductility. The built direction at a 45° angle had the worst tensile strength of all [55]. The hardness of material increases when the porosity is decreased [55]. Due to rapid cooling rate and small grain size, the SLM process can produce the final parts with higher micro harness than that of the conventional process (e.g. casting, forging, and welding) [46, 7]. In [52], they reported that the roughness on the top surface of parts will improve when using low hatch spacing with low scanning speed and higher laser power. One of the major problems of SLM final parts is residual stresses and distortion due to the temperature gradient in the process [20]. The residual stress is a stress within metal 3D printing parts that remain with the removal of the applied force [20]. The Island scanning pattern can reduce the porosity but lead to enhanced the residual stress. Smaller island scanning pattern presented the lower residual stress than larger island. In addition, the pre heating the substrate help reducing the residual stress [56]. The materials microstructure from SLM process generally consist of overlapped melted pool tracks with crystallized grains of cellular-columnar structure oriented according to thermal gradient direction. The cellular-columnar microstructure is typical solidified metal under rapid cooling rate and rapid solidification. [57].

RECENT CASE STUDIES OF SIMULATION IN METAL 3D PRINTING

Over the last decade, several researchers [58, 59, 60] have investigated and built numerical models to simulate the complex physics such as the heat transfer, molten fluid flow, melting solidification, melted track characteristic phenomena, residual stress, and parts performance in metal 3D printing technologies. This section will show and discuss the eight examples of metal 3D printing simulation case studies.

Case Study 1 Thermal Behavior in Selective Laser Melting (SLM) Process

Y. Li and D. Gu [61] have developed a 3D finite element (FE) model to study the effect of laser processing conditions on thermal behavior of pure titanium powder in selective laser melting (SLM) process. The study considers the temperature-dependent thermos physical parameters and the Gaussian distribution of the heat flux. The commercial computer simulation software ANSYS multiphysics FE package was used in the study. The 3D FE model used in the study with scanning pattern is shows in Fig. 16 (a). They found that: (1) the average temperature of the powder bed gradually increased during laser source scanning because of the heat accumulation, (2) the maximum temperature gradient in the molten pool increased slightly when the scanning speed was increased from 50 to 200 mm/s, but increased significantly when the laser power was increased from 100 to 200 W, (3) the width and depth of the melt pool decreased when scan speed was increased from 50 to 200 mm/s, (4) the microstructure was investigated to verify the reliability of the physical model and there was less balling and pore formation with laser power of 150 W and scanning speed of 100 mm/s which are the optimum condition for liquid formation and wettability in this case. Figure 16 (b), (c) shows an example temperature distribution during SLM process simulation with laser power of 100 W and scanning speed of 100 mm/s. Figure 17 shows the influence of the scanning speed (a), laser power (b) on the width and depth of the molten pool, and (c) an example of SEM images of surface morphology of SLM processed Ti sample with laser power of 150 W and scanning speed 100 mm/s.
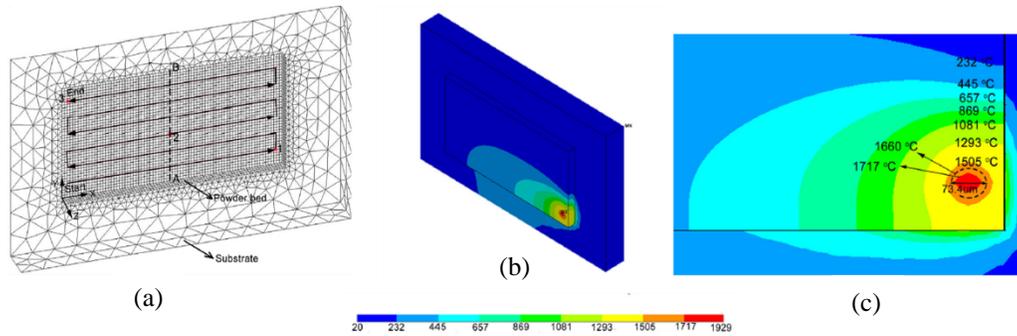
FIGURE 16. An example of temperature distribution during SLM process with laser power of 100 W and scanning speed of 100 mm/s [61].
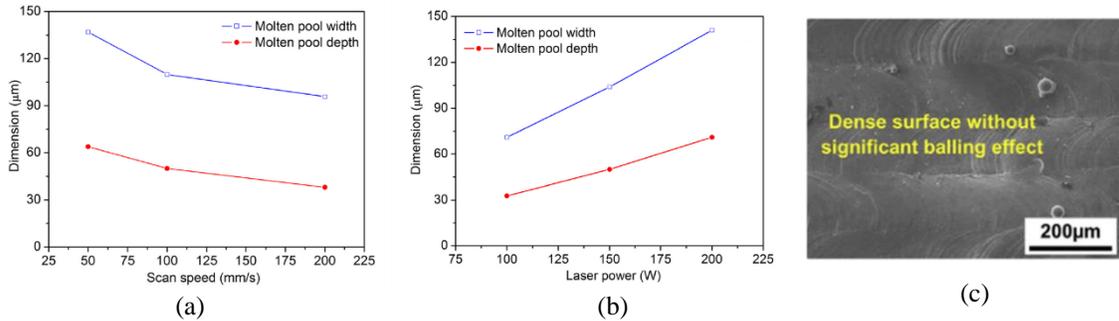

FIGURE 17. The influence of the scan speed (a) and laser power (b) on the width and depth of the molten pool. An example of SEM images of surface morphology of SLM processed Ti sample with laser power 150 W and scanning speed 100 mm/s (c) [61].

Case Study 2 Mesoscopic Simulation of Heat Transfer and Fluid Flow in SLM

Y.S. Lee and W. Zhang [23] solved the 3D transient numerical mesoscale model of Inconel 718 powder bed with a mesh size of 3 micron considering the volume of fluid method (VOF), particle size distribution and packing density. The numerical model is applied in order to understand the effect of laser power, scanning speed, powder size distribution, and powder packing characteristic on the balling effect formation in laser powder bed fusion

(SLM) process. The 3D powder bed simulation model was studied by CFD simulation software Flow-3D/Flow-weld. The research consists of two models in sequence. The first model, powder particle packing model, was solved by discrete element method (DEM), The second model, heat transfer and fluid flow model, was solved by finite difference method and volume of fluid (VOF) method. The 3D CAD model used in the study were powder layer with thickness of 50 μm on the substrate as shown in Fig. 18. Figure 19 presents the results of molten pool simulation with scanning speed of 1.1 m/s, laser power of 150 W and 45% packing density. From this study, they found that too fast scanning speed and too low laser power can increase the chance of discontinuous molten pool and the balling effect. The effect of particle size distribution on molten pool formed is shown in Fig. 20. Large particle size distribution causes the partial melting. This phenomenon occurs due to the higher mass and volume of particle. When using the small particle size distribution, the full melting can be formed.
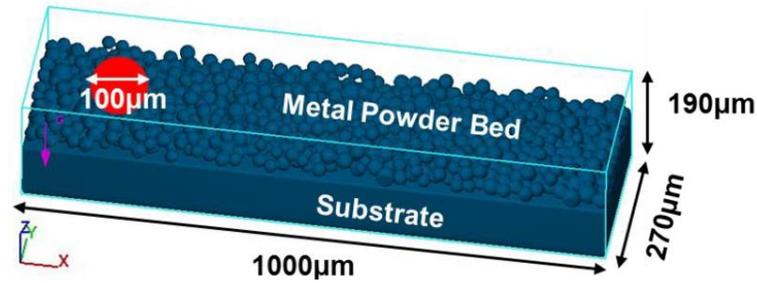
FIGURE 18. The 3D CAD model used in the study consists of powder layers with of thickness 50 μm on the substrate [23].
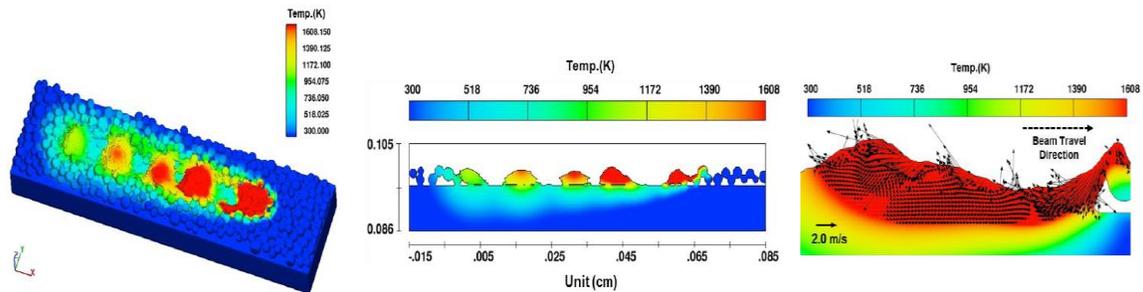
FIGURE 19. The results of molten pool simulation with scanning speed 1.1 m/s, laser power 150 W and packing density 45%.pool [23].
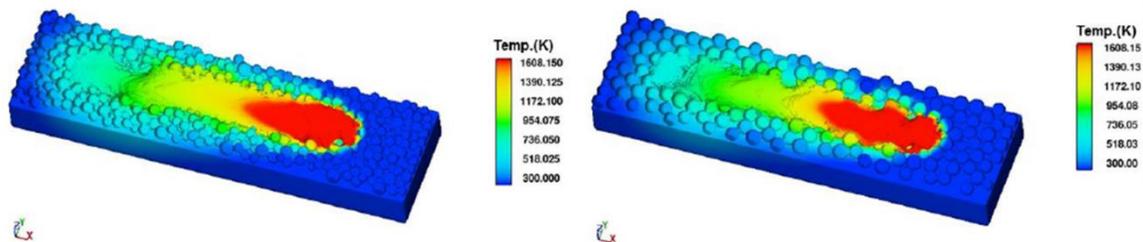
FIGURE 20. The effect of particle size distribution on molten pool formed [23].

Case Study 3 Temperature Distribution and Melt Pool Geometry in SLM Process

Ninpetch et. al. [35] studied the influence of process parameters on the melt pool geometry and single melted track characteristic of AISI 420 in the SLM process by using the commercial CFD software simulation, Flow-3D / Flow-weld. The results of the study were validated with the results from a previous research study [47]. Heat

transfer simulation model in SLM process consists of heat conduction, heat convection, and heat radiation The latent heat evolution arising from phase change during the tranformation from solid to liquid in the process can be applied in modelling [23]. The molten fluid flow simulation model of SLM process is based on numerical solution of mass, energy and momentum conservation, and the volume of fluid (VOF) method. The VOF is used to track the position and shape of the molten pool surface. The molten fluid flow is assumed to be incompressible and Newtonian with laminar. In the simulation, the Gaussian laser moving heat source model and a computational mesh of around 375,000 cells were used in this study. Table 2 presents the materials properties of AISI 420 stainless steel from Flow-3D database and process parameters used in this study.

TABLE 2. Materials properties of AISI 420 and Process parameters used in this simulation study [62].

Materials properties and process parameters	Value (unit)
Liquidus	1510 (^{o}C)
Solidus	1454 (^{o}C)
Latent heat of fusion	3.04 x 10^9 (J/kg)
Viscosity	0.05 (kg/m/s)
Laser power	120, 140 (Watt)
Scanning speed	0.4, 0.6, 0.8 (m/s)

The thermal-physical properties of AISI 420 martensitic used in the research including density, thermal conductivity, and specific heat are plotted in Fig. 21 [62].
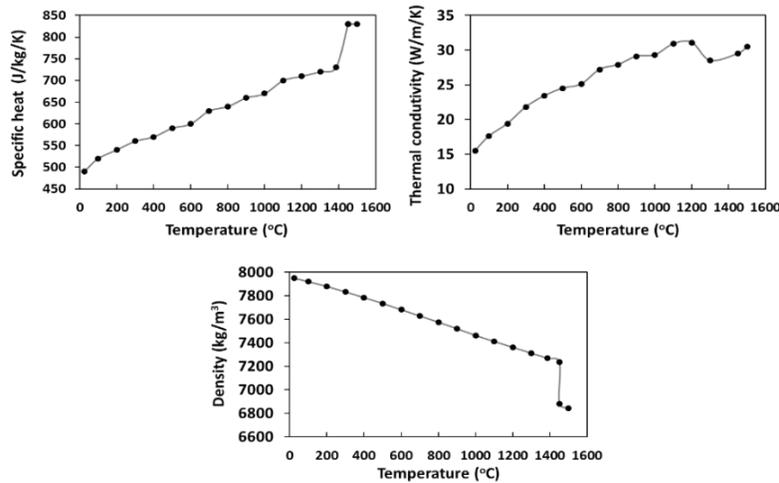

FIGURE 21. Thermal-physical properties of AISI 420 stainless steel including density, thermal conductivity, specific heat [62].

From the study, the results show that when the scanning speed increase, the geometry of melt pools can be tranformed from ellipse shape to tear drop shape as shown in Fig. 22. Melt pool geometry can determine the density, porosity and surface roughness of final products. Figure 23 shows the longitudinal section view of molten metal pool, which is parallel to the laser scanning direction. The temperature distribution and velocity flow field are plotted as the color contours and the arrows. The molten metal pool boundary is presented in red color at 1600 ^{o}C, which is the melting temperature of steels. The surface tension at the center of melt pool is lower than the back region of molten metal pool, thereby leading to the backward flow of the molten metal near the surface. The surface tension will induce the Marangoni flow from lower surface tension region to higher surface tension region.
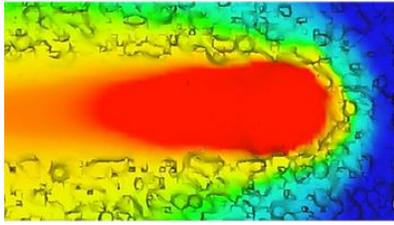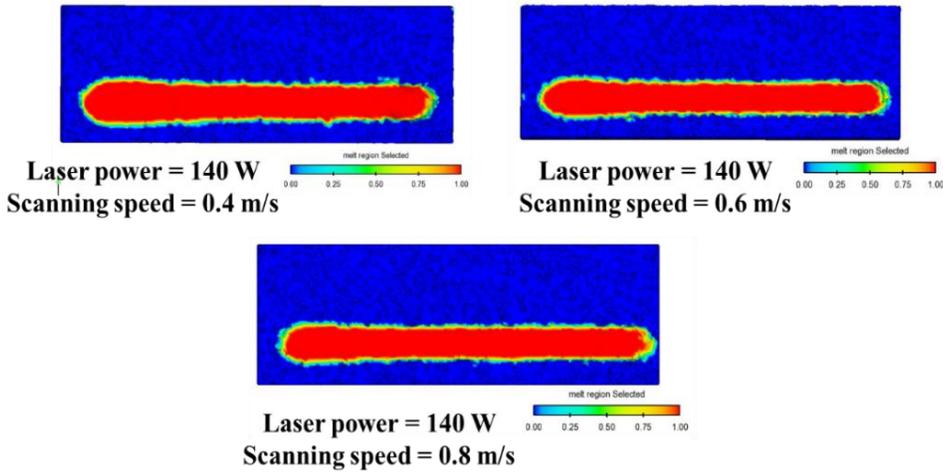
Laser power = 120 W
Scanning speed = 0.4 m/s
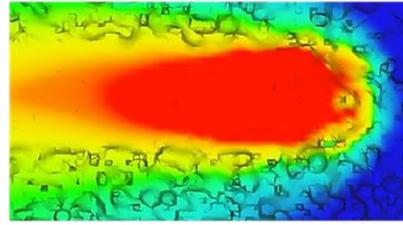
Laser power = 120 W
Scanning speed = 0.6 m/s

FIGURE 23. Longitudinal section view of molten metal pool and fluid flow in molten metal pool [35].

Figure 24 and 25 present the effects of scanning speed on single track formation width and depth. The width and depth of single melted track formation are increased when lower scanning speed is applied. The results from the simulation is in agreement with the experimental results as shown in Fig. 26 (a).

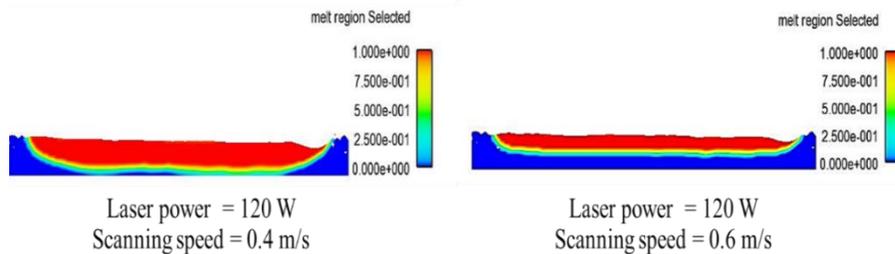Laser power = 140 W
Scanning speed = 0.4 m/s

Laser power = 140 W
Scanning speed = 0.6 m/s

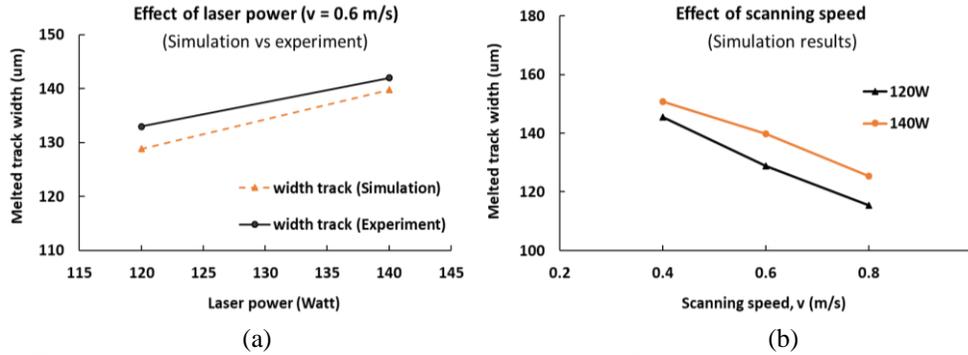Laser power = 140 W
Scanning speed = 0.8 m/s

FIGURE 24. The effect of scanning speed on the width of single-track formation [35].

Laser power = 120 W
Scanning speed = 0.4 m/s

Laser power = 120 W
Scanning speed = 0.6 m/s

FIGURE 25. The effect of scanning speed on single track formation depth [35].

FIGURE 26. The simulation results validated with experimental results (a), The effect of process parameter on the width of single track formation [35].

Case Study 4 Multi-Scale and Multiphysics Modelling in SLM Process

N. P. Lavery et.al [63] developed a computational modelling of the powder melting at microscale in additive layer manufacturing. This simulation model comprises of melting and solidification based on the enthalpy-porosity method, free surface, multiple phase (e.g. solid, liquid, and gas), force and natural convection of argon gas, laser beam energy source, material properties with temperature dependent, and surface tension. In the study, discrete ordinate radiative heat transfer model in FLUENT using User Defined Functions (UDFs) was applied to design the laser source moving along the top boundary. A three-powder layer modelling on substrate was used as a geometry model. The process parameters used the study include laser power of 200 W with the focal diameter size of 70 μm, and the powder particle size of 70 μm respectively. Figure 27 shows the melt pool modelling by using FLUENT software.
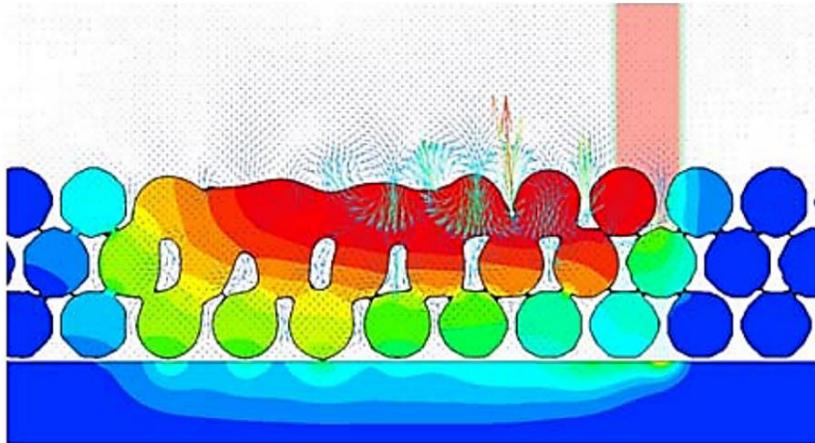
FIGURE 27. The melt pool modelling using FLUENT software [63].

Case Study 5 Physical Phenomena of Refractory Metals in SLM Process

K.-H. Leitz [64] studied physical phenomena of refractory metals in selective laser melting process by using COMSOL Multiphysics with Computational Fluid Dynamics and the Heat Transfer module of finite element simulation software package. The numerical model consists of laser absorption on the metal surface, conductive and convective in the metal and the ambient atmosphere, melting, solidification, and evaporation. The example of simulation model for SLM is shown in Fig. 28. In this study, multiphysical modelling was used to analyze the influence of process parameters on physical phenomena and melted track characteristic of refractory metals (e.g. Steel and Molybdenum). The geometry model used in the study consists of a powder layer on a substrate plate. It was found that the melt pool occurs when laser radiation is absorbed on the surface of the metal powder. For steel,

the long melt pool with evaporation can be formed during the SLM process. Whereas, the size melt pool of molybdenum is small without evaporation due to the high thermal conductivity of material. Figure 29 present the melted pool and molten fluid flow characteristic of (a) steel powder bed and (b) molybdenum powder bed in SLM process.
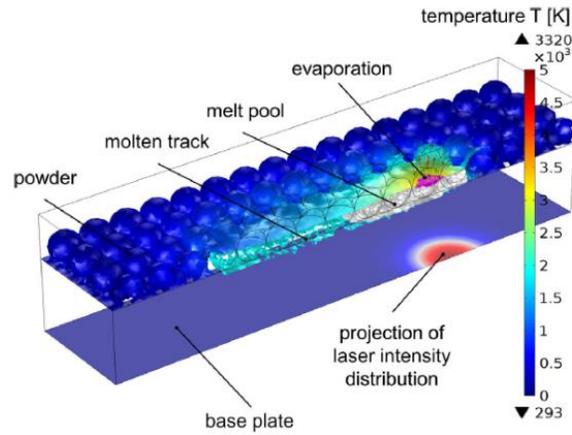
FIGURE 28. The example of simulation model for SLM [64].
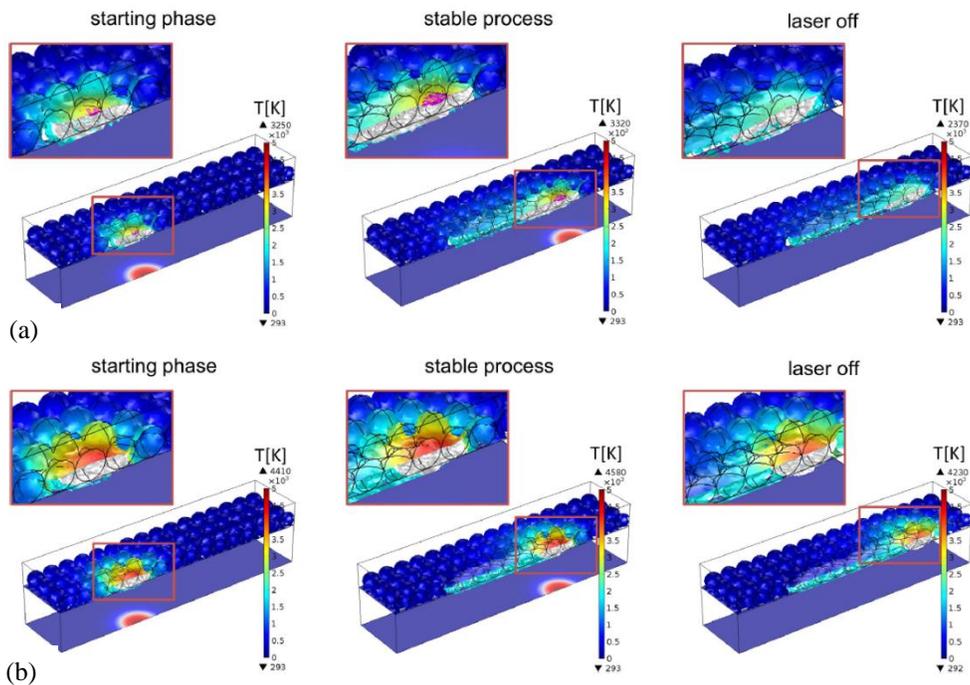
FIGURE 29. Molten fluid flow characteristic of (a) steel, (b)molybdenum powder bed in SLM process [64].

Case Study 6 Parametric Study of Surface Morphology for Selective Laser Melting (SLM) Process

Y.C. Wu et al. [65] developed a three-dimensional (3D) numerical model to investigate the effect of process parameter, scanning speed, on the surface morphology of Ti-6Al-4V powder bed in selective laser melting (SLM) process with numerical and experimental method. The surface morphology can be obtained from free surface of melt

pool which is calculated by the Volume of fluid (VOF) method. Figure 30 (a) presents the simulation model which consist of the Ti-6Al-4V powder bed with particle size of 35 μm and the Ti-6Al-4V bulk for substrate. The numerical simulation was performed by commercial CFD simulation software flow-3D. To evaluate the surface morphology, firstly, the surface contour obtained by simulation and experimental study were divided into fifteen points equally as shown in Fig. 30 (b). Then, the melted track heights at each point were measured to finally calculate the surface variation by using Equation (1).

(a)

(b)
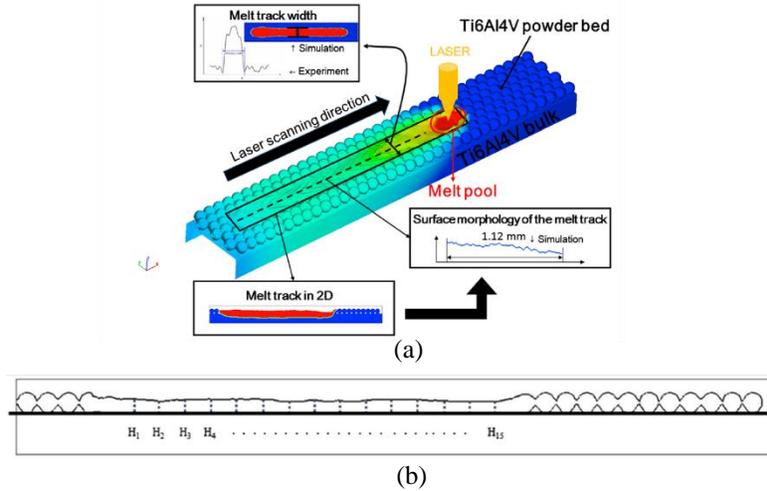
FIGURE 30. (a) simulation model, (b) The assessment of surface morphology from simulation result [65].

The surface variation is described as follows:

$$\text{Surface variation} = \sqrt{\frac{\sum_{i=1}^{15}\left(H_i - H_{avg}\right)^2}{15}} \qquad (1)$$

where H_i is the height from each divided point of the melt track, and H_{avg} is the average height.

From the study, they discovered that the flat surface morphology can be obtained when higher scanning speed is applied as shown in Fig. 31 (a). Figure 31 (b) presents the results from the simulation is in agreement with the experimental results.

(a)

(b)
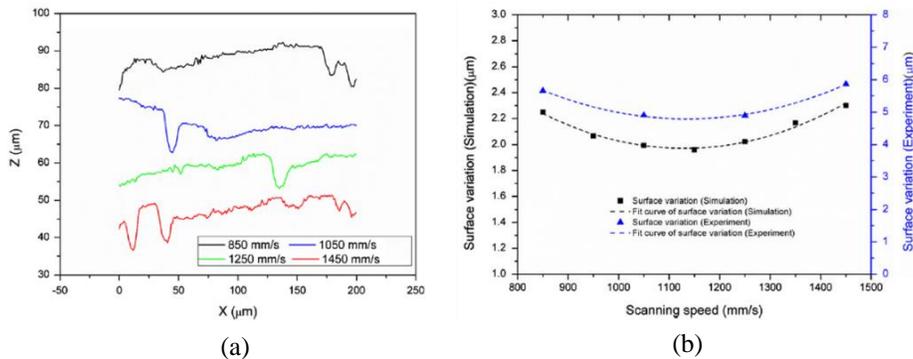
FIGURE 31. (a) surface morphology with varied scanning speed, (b) simulation and experiment result of Surface variation [65].

Case Study 7 Multi-Track Simulation of Electron Beam Melting (EBM) Process

W. Yan et.al [66] developed the multi-track simulation of electron beam melting (EBM) process to investigate the influence of scanning path and hatching distance on layer formation. The scanning path is one of the significant laser process parameters to create full dense parts and smooth surface. The two types of the scanning path used in the study were (a) Z-shaped and (b) S-shaped as shown in Fig. 32. The hatching distance (distance between two neighboring tracks) were set to 0.2, 0.24, 0.26, and 0.32 mm respectively. The material used in the study was Ti-6Al-4V powder. The laser power of 60 W and scanning speed of 0.5 m/s were applied in the study.
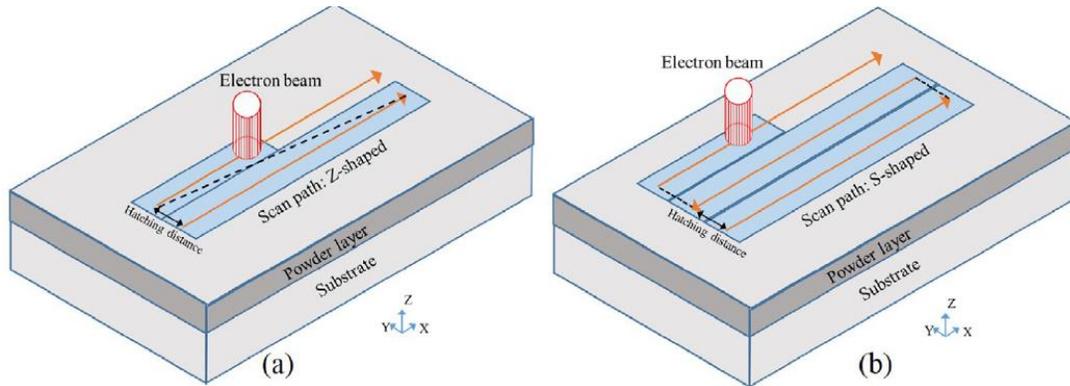
FIGURE 32. The two type of scanning path used in the including (a) Z-shaped and (b) S-shaped [66].

In Fig. 33 (a), (b), (c), and (d), the cross section of layer formation with different hatching distance at a given x position of 0.35 mm, 1.04 mm and 2.06 mm are displayed. The red color contour shows the melt region and the blue color presents solid or unmelt region. In the cross sectional microstructure, the effect of hatching distance can be observed more clearly. When the gap between two neighboring tracks is increased, the separation with an increase of hatching distance occurs.
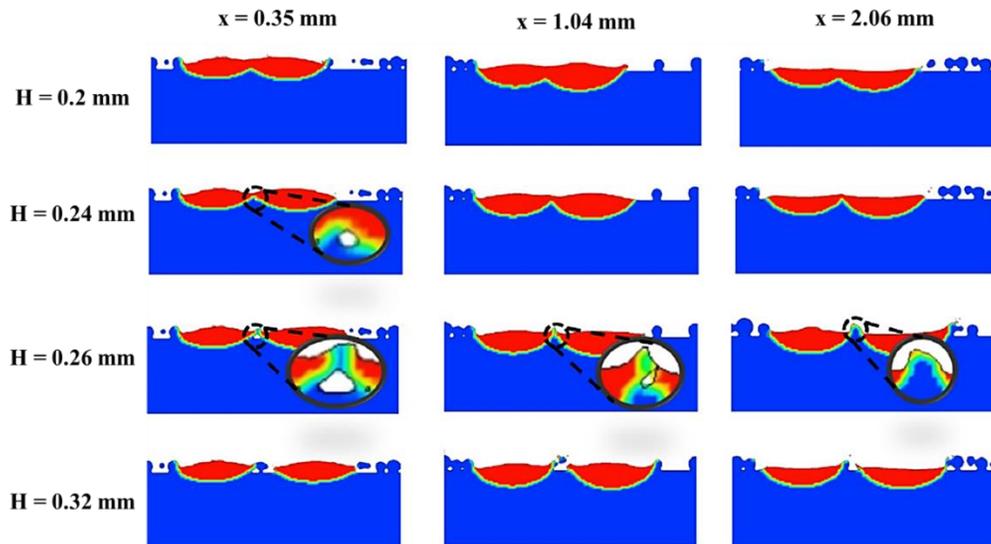
FIGURE 33. (a), (b), (c), and (d) the cross section of layer formation with different hatching distance at a given x position of 0.35 mm, 1.04 mm and 2.06 mm [66].

Case Study 8 Thermal-Mechanical Behavior Modelling

L. V. Belle [24] investigated the numerical simulation of complex shape part, turbine, fabricated by selective laser melting (SLM) process. This numerical modelling based on finite element method (FEM) which are used to study and predict the residual stress and distortion. Figure 34 illustrates the turbine geometry with fifteen sliced layers used for the investigation. The layer thickness of each layers is 40 µm. The mesh of around 2.6×10^6 elements was used in the study. The thermal condition in the numerical modelling consists of (1) heat transfer between the bottom face of building platform and the additive manufacturing machine platform and (2) heat transfer between another face and powder bed. The initial temperature was 40°C. For mechanical condition, the bottom face displacement of building platform was set to block in vertical direction. The material used in the study was maraging steel. The procedure of this numerical study was firstly started with building the first sliced layer at a temperature of 1400°C. Then, the next sliced layers were repeatedly built one by one until all part layers are completed.

Activation of the 10th layer
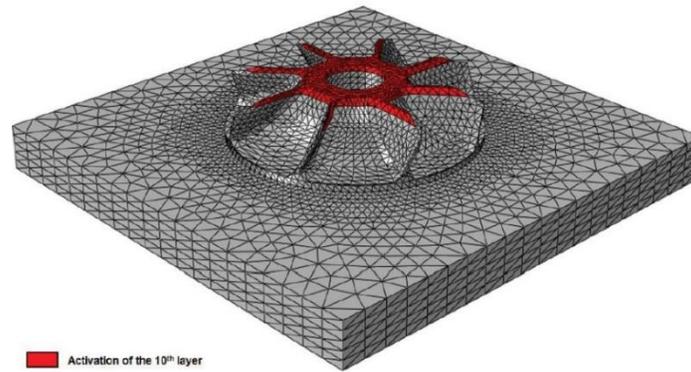
FIGURE 34. The turbine geometry formed fifteen sliced layers [24].

From simulation results of this study, it was found that, (1) due to heat accumulation and reducing the thermal gradients, the residual stress is slightly lower on the top surface of the turbine as shown in Fig. 35 (a), (2) the value of Von Mise stress reached 1200 MPa, which is close to the strength of maraging steel at room temperature, and (3) distortions reached 0.8 mm at the edge of turbine blades, as shown in Fig. 35 (b).

(a)   (b)
FIGURE 35. Residual stresses and distortions field of the turbine complex part [24].

TABLE 3. Numerical Simulation model from literature review

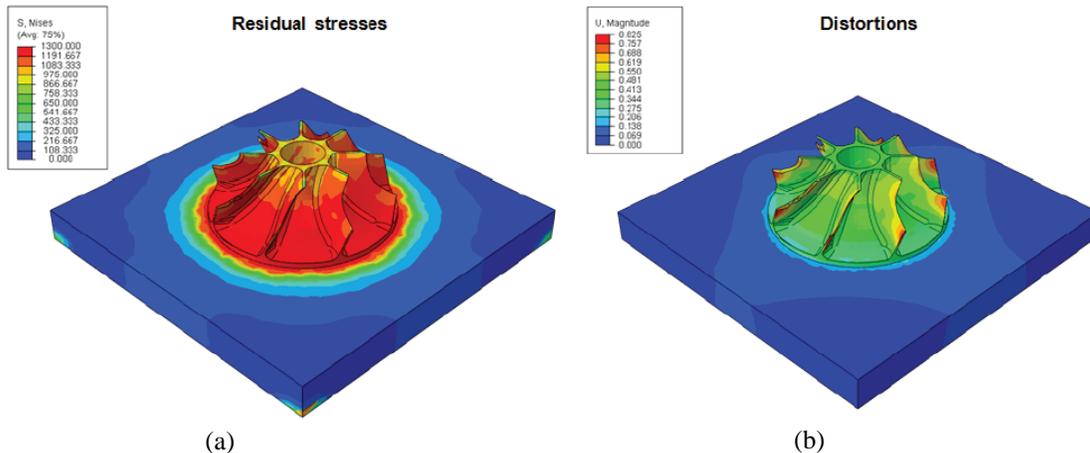| Material	Process	Process Parameters				References
		Laser power (W)	Scanning speed (mm/s)	Laser spot size (mm)	Hatch spacing (mm)	
Inconel 718	SLM	100-300	200-2,5000	N/A	N/A	67
AISI 316L	SLM	210	12.7	0.9	N/A	68
Hot work steel (AISI H13)	SLM	175	740	0.07	N/A	69
Ti-6Al-4V	EBM	120-360	100-1,000	0.4-1.0	N/A	70
Ti-6Al-4V	EBM	30-90	500	0.2	0.2-0.32	66
Titanium	SLM	100-200	50-200	0.1	0.05	61
Inconel 718	DMLS/EBM	185-500	1,200-5,000	N/A	0.1-0.18	36
AlSi10Mg	SLM	150-300	100-400	0.07	0.05	71
Ti-6Al-4V	SLM	140-210	850-1450	0.035	N/A	65
Steel	LBM	200	1000	0.1	0.1	72
AISI 316L	SLM	50-400	750-6,000	0.027	N/A	73
Inconel 625	SLM	195	N/A	0.1	0.1	74
Inconel 718	SLM	150-200	1.1- 2.3	0.1	N/A	23
AISI 420	SLM	120-140	400-800	0.08	N/A	35

SUMMARY AND CONCLUSIONS

In this paper, the review a computer simulation of metal 3D printing can be summarized as follows: (1) The numerical modelling and computer simulation are useful for investigation and prediction of the underlying physical phenomena, and thermal-mechanical behavior that can occur during the metal 3D printing process, (2) The numerical modelling can now support various types of the metal 3D printing process such as selective laser melting (SLM), direct metal laser sintering (DMLS), direct energy deposition, and electron beam melting (EBM), (3) the Computer simulation modelling in metal 3D printing has been classified into four levels including micro-scale (10^{-9} m to 10^{-6} m), particle scale (10^{-6} m to 10^{-3} m), meso-scale (10^{-3} m), and macro-scale (10^{-3} m to 1 m), to explain several aspects of the process, and (4) the simulation software is a valuable tool to gain the body of knowledge of several aspects in the metal 3D printing technologies. Additionally, the authors' future work will be focused on the numerical modelling of multiple track formation (layers) and multi-layers powder bed of medical materials Ti-6Al-4V alloys to investigate and improve the metal 3D printing process for implantable medical device applications. The results from the future work will be beneficial to the development of Thailand's implantable medical device quality.

ACKNOWLEDGEMENT

REFERENCES

1. B. Berman, Bus Horizons **5**, 155-162 (2012)
2. ASTM Standard F-2792-12a. Standard Terminology for Additive Manufacturing Technologies, ASTM International
3. D. L. Bourell, M.C. Leu, J. J. Beaman and D.W. Rosen, A Brief History of Additive Manufacturing and the 2009 Roadmap for Additive Manufacturing: Looking Back and Looking Ahead, US – TURKEY Workshop on Rapid Technologies, 2009, pp. 5-11.
4. T. Wohlers, Additive Manufacturing State of the Industry, Wohlers report, 2010, pp. 1-26.
5. V. Bhavar, P. Kattire, V. Patil, S. Khot, K. Gujar and R. Singh, A Review on Powder Bed Fusion Technology of Metal Additive Manufacturing, International conference and exhibition on Additive Manufacturing Technologies-AM-2014, Banglore, India, 2014.
6. D. Thomas, The Development of Design Rules for Selective Laser Melting, Ph. D Thesis University of Wales Institute Cardiff, 2009.
7. P. Eriksson, Evaluation of mechanical and microstructural properties for laser powder-bed fusion 316L, Uppsala university, 2018.
8. CNC vs 3D printing, https://www.3dnatives.com/en/3d-printing-vs-cnc-160320184/cnc-vs-3d-4, (accessed on 2 March 2019).
9. W. E. Frazier, Journal of Materials Engineering and Performance **23** 1917-1928 (2014)
10. Characterizing metal powders for additive, https://www.materials-talks.com/blog/2018/11/28/analytical-tools-for-characterizing-metal-powders-for-additive-manufacturing/ (accessed on 9 April 2019).
11. M. Yakouta, M. A. Elbestawi and S. C. Veldhuis, Solid State Phenomena **278**, 1-14 (2018)
12. T. D. Ngoa, A. Kashania, G. Imbalzanoa, K.T.Q. Nguyena, and D. Huib, Composites Part B **143**, 172-196 (2018)
13. Metal 3D Printing Technology, https://creatz3d.com.sg/metal-3d-printers (accessed on 2 April 2019).
14. Binder Jetting 3D Printing, https://3dsourced.com/3d-printing /binder-jetting/ (accessed on 9 March 2019).
15. High Level Processes: Directed Energy Deposition, https://www.bintoa.com/DED (accessed on 5 April 2019).
16. Matthias Markl and Carolin Korner, Multi-Scale Modeling of Powder-Bed-Based Additive Manufacturing, Annual Review of Materials Research 2016, Vol. 46, pp. 1-34.
17. P. Keane, 3D Printing Simulation, Part 1: Where Are We Now, https://www.engineering.com/ Simulation, (accessed on 10 May 2019).
18. 3D Printer Simulator – A Short Guide to 3D Printing Simulations, https://all3dp.com/1/best-free-3d-printing-software-3d-printer-program/ (accessed on 10 May 2019).
19. Ten companies Offering Cutting-Edge 3D Printing Simulation Software, https://amfg.ai/2018/09/20/10-companies-offering-cutting-edge-simulation-3d-printing-software/, (accessed on 10 May 2019).
20. W. J. Sames, F. A. List, S. Pannala, R. R. Dehoff, and S. S. Babu, The metallurgy and processing science of metal additive manufacturing, International Materials Reviews, 2016, pp. 1-47.
21. C.A. Gandin, C.R. Phys. **11**, 216-225 (2010)
22. Ch. Panwisawas, Ch. Qiu, M. J. Anderson, Y. Sovani, Ri. P. Turner, M. M. Attallah, J. W. Brooks, H. C. Basoalto, Computational Materials Science **126**, 479-490 (2017)
23. Y. S. Lee and W. Zhang, Mesoscopic Simulation of Heat Transfer and Fluid Flow in Laser Powder Bed Additive Manufacturing, International Solid Free Form Fabrication Symposium Austin, 2015, pp. 1154-1165.
24. L. V. Belle, Numerical simulation of complex part manufactured by Selective Laser Melting process, Proceedings of the 20th International ESAFORM Conference on Material Forming AIP Conf. Proc. Vol. 1896, pp. 040013-1–040013-5.

25. B. Radhakrishnan, S. Gorti and S. S. Babu, Large scale phase field simulations of microstructure evolution during thermal cycling of Ti–6Al–4V, Proceeding of International Conference on Solid-Solid Phase Transformations in Inorganic Materials (PTM) Whistler, Canada, 2015.
26. A. Zinoviev, O. Zinovieva, V. Ploshikhina, V. Romanova, R. Balokhonov, Materials and Design **106**, 321-329 (2016)
27. W. Yan, S. Lin, O. L. Kafka, Y. Lian, Ch. Yu, Z. Liu, J. Yan, S. Wolff, H. Wu, E. Ndip-Agbor, M. Mozaffar, K. Ehmann, J. Cao1, G. J. Wagner, W. K. Liu, Computational Mechanics, **61**, 521-541 (2018)
28. J. C. Steuben, A. P. Iliopoulos, J. G. Michopoulos, Computer Methods in Applied Mechanics and Engineering **305**, 537-561 (2016)
29. K. Carolin, B. Andreas and E. Attar, Model Simul Mater Sci Eng **21**, 1-18 (2013)
30. K. Alexander, B. Andreas and K. Carolin, Journal of Physics D: Applied Physics **47**, 1-11 (2014)
31. K. Zeng, D. Pal and B. Stucker, Proceedings of Solid Freeform Fabrication Symposium Austin **60**, 796-814 (2012)
32. H. S. Carslaw and J. C. Jaeger, Conduction of Heat in Solids, Oxford University Press, Amen House London E.C., 1959.
33. B. Xiao and Y. Zhang, Numerical Heat Transfer, **51**, 715-733 (2007)
34. Y. Zhang, A. Faghri, C. W. Buckley and T. L. Bergman, Transactions of the ASME **122**, 150-158 (2000)
35. P. Ninpetch, P. Kowitwarangkul, S. Mahathanabodee, R. Tongsri, and P. Ratanadecho, Thermal and Melting track Simulations of Laser Powder Bed Fusion (SLM), Proceeding of International Conference on Materials Research and innovation (ICMARI), Bangkok, Thailand, 2018, (in press)
36. P. Prabhakar, W.J. Sames, R. Dehoff, S.S. Babu, Additive Manufacturing **7**, 83-91 (2015)
37. M. Orme, I. Madera, M. Gschweitl, and M. Ferrari, Designs **2**,1-22 (2018)
38. Topology optimisation for 3D printing, https://www.3dnatives.com/en/topology-optimisation, (accessed on 10 July 2019).
39. Space claim & Topology optimization, https://twitter.com/spaceclaim/status/696773365751799808, (accessed on 10 July 2019).
40. J. P. Choi, G. H. Shin, M. Brochu, Y. J. Kim, S. S. Yang, K. T. Kim, D. Y. Yang, Ch. W. Lee, and J. H. Yu, Materials Transactions **57**, 1952 -1959 (2016)
41. N. T. Aboulkhaira,, N. M. Everitta, I. Ashcroftb, Ch. Tuck, , Additive Manufacturing **1**, 77-86 (2014)
42. R. Li, J.Liu, Y. Shi, M. Z. Du, and Z. Xie, Journal of Materials Engineering and Performance **19**, 666–671 (2010)
43. P. Bidare, R.R.J. Maier, R.J. Beck, J.D. Shephard, A.J. Moore, Additive Manufacturing **16**, 177–185 (2017)
44. K. Saeidi, Stainless steel fabricated by laser melting, Doctoral Thesis Stockholm University, 2016.
45. S. David and J. Vitek, Principle of Weld solidification and Microstructure, International trends in Welding Science and Technology, ASM, 1993, pp. 147-157.
46. P. Ninpetch, P. Kowitwarangkul, S. Mahathanabodee, R. Tongsri, and P. Ratanadecho, The Influence of Laser Parameters on the Melted Track and Microstructure of AISI 316L Fabricated by SLM process, Proceedings of the 8th Asia Pacific IIW international conference congress, Bangkok, Thailand, 2019, IIWAP2019-A03, pp. 39-44
47. X. Zhao, Q. Wei, B. Song, Y. Liu, X. Luo, S. Wen, and Y. Shi, Fabrication and Characterization of AISI 420 Stainless Steel Using Selective Laser Melting, Materials and Manufacturing Processes, 2015, pp. 1–7.
48. I. Yadroitsev, and I. Smurov, Physics Procedia **5**, 551-560 (2010)
49. Y. Guo, L. Jia, B. Kong, N. Wang, and H. Zhang, Chinese Journal of Aeronautics **31**, 860-866 (2018)
50. R. Li, J. Liu, Y. Shi, L. Wang, and W. Jiang, International Journal of Advanced Manufacturing Technology **59**, 1025-1035 (2012)
51. M. H. Hong, B. K. M, and T. Y. Kwon, Appl. Sci **6**, 1-10 (2016)
52. I. Yadroitsev, and I. Smurov, Physics Procedia **12**, 264-270 (2011)
53. P.Hanzl, M. Zetek, T. Bakša, T. Kroupa, Procedia Engineering **100**, 1405-1413 (2015)
54. K. Guan, Z. Wang, M. Gao, X. Li, X. Zeng, Materials and Design, **50**, 581-586 (2013)
55. J. A. Cherry, M. Davies, S. Mehmood, N. P. Lavery, S. G. R. Brown, J. Sienz, International Journal of Advanced Manufacturing Technology **76**, 869–879 (2015)
56. A. Wu, M. M. LeBlanc, M. Kumar, G. F. Gallegos, D. W. Brown and W. E. King: 'Effect of laser scanning pattern and build direction in additive manufacturing on anisotropy, porosity and residual stress', in '2014 TMS annual meeting & exhibition', San Diego, CA, 2014.
57. Z. Brytan, Arch. Metall. Mater **62**, 2125-2131 (2017)

58. B. Xiao and Y. Zhang, Numerical Heat Transfer **51**, 715-733 (2007)
59. W. L. Chen, Y. C. Yang and H. L. Lee, Estimating the absorptivity in laser processing by inverse methodology, Applied Mathematics and Computation, 2007, pp. 712-721.
60. C. Konrad, Y. Zhang, and B. xiao, Analysis of melting and resolidification in a two-component metal powder bed subjected to temporal Gaussian heat flux, International Journal of Heat and Mass Transfer, 2005, pp. 3932-3944.
61. Y. Li and D. Gu, Additive Manufacturing **1**, 99-109 (2014)
62. Flow3d: Version 11.0.1.2 (2014): User manual, Flow science, Santa Fe, NM, USA.
63. N. P. Lavery, S. G. R. Brown, J. Sienz, J. Cherry and F. Belblidia, A review of Computational Modelling Additive Layer Manufacturing – multi-scale and multi-physics, Design and Manufacturing, 2014, pp. 668-690.
64. K.H. Leitz, P. Singer, A. Plankensteiner, B. Tabernig, H. Kestler, and L.S. Sigl, Metal Powder Report **72**, 333-338 (2017)
65. Y. Ch. Wu, W.S. Hwang, C.H. San, C. H. Chang, and H.J. Lin, Parametric study of surface morphology for selective laser melting on Ti6Al4V powder bed with numerical and experimental methods, International Journal of Material Forming, 2017, pp. 1-7.
66. W. Yan, W. Ge, Y. Qian, S. Lin, B. Zhou, W. K. Liu, F. Lin, G. J. Wagner, Acta Materialia **134**, 324-333 (2017)
67. R. Andreotta, L. Ladani, W. Brindley, Finite Elements in Analysis and Design **135**, 36-43 (2017)
68. V. Manvatkar, A. De, and T. DebRoy, Journal of Applied Physics **116**, 124905-1-124905-8 (2014)
69. J. Zielinski, S. Vervoort, H. W. Mindt, and M. Megahe, BHM **162**, 192-198 (2017)
70. S.A. Khairallah, A. T. Anderson, A. Rubenchik, and W. E. King, Acta Materialia **108**, 36-45 (2016)
71. Y. Li and D. Gu, Materials and Design **63**, 856-867 (2014)
72. F.-J. Gürtler, M. Karga, K.-H. Leitza, and M. Schmidt, Physics Procedia **41**, 881-886 (2013)
73. C. Tang, J. L. Tan, C.H. Wonga, International Journal of Heat and Mass Transfer **126**, 957-968 (2018)
74. S. Shrestha and K. Chou, Computational Analysis of Thermo-Fluid Dynamics with Metallic Powder in SLM, CFD Modeling and Simulation in Materials Processing, 2018, pp. 85-95.